

## An Ultra Metal-poor Star Near the Hydrogen-burning Limit\*

KEVIN C. SCHLAUFMAN,<sup>1</sup> IAN B. THOMPSON,<sup>2</sup> AND ANDREW R. CASEY<sup>3,4</sup>

<sup>1</sup>*Department of Physics and Astronomy*

*Johns Hopkins University  
3400 North Charles Street  
Baltimore, MD 21218, USA*

<sup>2</sup>*Carnegie Observatories  
813 Santa Barbara Street  
Pasadena, CA 91101, USA*

<sup>3</sup>*School of Physics & Astronomy  
Monash University*

*Clayton 3800, Victoria, Australia*

<sup>4</sup>*Faculty of Information Technology  
Monash University  
Clayton 3800, Victoria, Australia*

(Received 2018 August 6; Revised 2018 August 17; Accepted 2018 August 27)

ApJ in press

### ABSTRACT

It is unknown whether or not low-mass stars can form at low metallicity. While theoretical simulations of Population III (Pop III) star formation show that protostellar disks can fragment, it is impossible for those simulations to discern if those fragments survive as low-mass stars. We report the discovery of a low-mass star on a circular orbit with orbital period  $P = 34.757 \pm 0.010$  days in the ultra metal-poor (UMP) single-lined spectroscopic binary system 2MASS J18082002–5104378. The secondary star 2MASS J18082002–5104378 B has a mass  $M_2 = 0.14^{+0.06}_{-0.01} M_\odot$ , placing it near the hydrogen-burning limit for its composition. The 2MASS J18082002–5104378 system is on a thin disk orbit as well, making it the most metal-poor thin disk star system by a considerable margin. The discovery of 2MASS J18082002–5104378 B confirms the existence of low-mass UMP stars and its short orbital period shows that fragmentation in metal-poor protostellar disks can lead to the formation and survival of low-mass stars. We use scaling relations for the typical fragment mass and migration time along with published models of protostellar disks around both UMP and primordial composition stars to explore the formation of low-mass Pop III stars via disk fragmentation. We find evidence that the survival of low-mass secondaries around solar-mass UMP primaries implies the survival of solar-mass secondaries around Pop III primaries with masses  $10 M_\odot \lesssim M_* \lesssim 100 M_\odot$ . If true, this inference suggests that solar-mass Pop III stars formed via disk fragmentation could survive to the present day.

*Keywords:* binaries: spectroscopic — Galaxy: disk — stars: formation — stars: low-mass — stars: Population II — stars: Population III

### 1. INTRODUCTION

The first stars in the universe—the so called Population III (Pop III) stars<sup>1</sup>—are unique in that they are composed exclusively of the stable products of big bang nucleosynthesis: hydrogen, helium, and a dusting of

Corresponding author: Kevin C. Schlafman  
kschlaufman@jhu.edu

\* This paper includes data gathered with the 6.5 meter Magellan Telescopes located at Las Campanas Observatory, Chile.

<sup>1</sup> The current state of Pop III star formation research is reviewed in Bromm (2013), Glover (2013), and Greif (2015).

lithium (e.g., Alpher et al. 1948; Cyburt et al. 2016). Unlike metal-enriched gas that efficiently cools via dust and metal-line emission, metal-free gas can only cool significantly via atomic (H), molecular ( $\text{H}_2$ ), and deuterated (HD) hydrogen emission. Hydrogen can only cool gas down to temperatures  $T \lesssim 10^4$  K, and  $\text{H}_2$  is a poor coolant at  $T \lesssim 200$  K. While HD can cool gas below  $T \approx 200$  K, the small cosmological ratio of deuterium to hydrogen limits its contribution to cooling. The net result is that primordial composition gas cannot efficiently cool, and this inefficient cooling implies large Jeans masses and therefore only massive star formation. Both simple models and the earliest cosmologically self-consistent three-dimensional hydrodynamic simulations of Pop III star formation supported this picture and suggested a characteristic Pop III star mass  $M_* \gtrsim 100 M_\odot$  (e.g., Silk 1983; Tegmark et al. 1997; Bromm et al. 1999, 2002; Abel et al. 2000, 2002; Yoshida et al. 2006; O’Shea & Norman 2007). These first-generation hydrodynamic simulations also indicated that Pop III stars should form as single stars in isolation.

These first-generation simulations did not include the effect of radiative feedback from the forming star. It has subsequently been shown that radiative feedback plays a critical role in halting accretion onto a Pop III star and consequently in setting its final mass (e.g., McKee & Tan 2008; Hosokawa et al. 2011; Stacy et al. 2012; Susa 2013; Hosokawa et al. 2016). The most recent simulations predict that Pop III stars should form over a range in mass  $10 M_\odot \lesssim M_* \lesssim 1000 M_\odot$ . This wide range in mass is a result of the varying far-ultraviolet background due to the expansion of the universe and the change in the characteristic mass of Pop III stars with time (e.g., Hirano et al. 2014, 2015; Susa et al. 2014). At the low-mass end, these theoretical predictions are supported by nucleosynthesis calculations that suggest that the relative abundances of metals observed in the most metal-poor stars are best explained by the supernovae of stars with initial masses in the range  $10 M_\odot \lesssim M_* \lesssim 100 M_\odot$  (e.g., Tumlinson 2006; Takahashi et al. 2014; Tominaga et al. 2014; Placco et al. 2015; de Bennassuti et al. 2017; Fraser et al. 2017; Ishigaki et al. 2018). The abundances expected from the pair-instability supernovae of Pop III stars with  $M_* \gtrsim 100 M_\odot$  are rarely seen, and this may suggest that the characteristic mass scale of Pop III stars is  $M_* \lesssim 100 M_\odot$  (e.g., Aoki et al. 2014; Takahashi et al. 2018).

While the observed chemical abundances of metal-poor stars can be used to constrain the properties of massive Pop III stars that explode as supernovae, they have nothing to say about the existence of low-mass Pop III stars. This is a major problem, as fragmentation at

the molecular core and protostellar disk scales has now been seen in numerical simulations of Pop III star formation (e.g., Clark et al. 2008, 2011a,b; Turk et al. 2009; Stacy et al. 2010, 2012, 2016; Greif et al. 2011, 2012; Dopcke et al. 2013; Stacy & Bromm 2013, 2014; Hirano & Bromm 2017; Riaz et al. 2018). Whereas fragmentation at the molecular core scale will likely lead to massive binary stars, the emergence of gravitationally bound solar-mass clumps in protostellar disks via gravitational instability has the potential to produce low-mass Pop III stars that may be observable in the Milky Way.

Even though the reality of fragmentation is now widely accepted, it is impossible to run these simulations forward in time long enough to evaluate whether or not these fragments will survive as low-mass stars or migrate inward and merge with the primary forming at the center of the system (e.g., Vorobyov et al. 2013). Consequently, it is still unknown whether or not low-mass Pop III stars ever existed. Despite decades of searching, no low-mass primordial composition star has ever been found. While it is possible to set upper limits on the occurrence of low-mass Pop III stars in the Milky Way, the heterogeneous nature and singular focus on the most metal-poor objects in the course of most metal-poor star surveys render them very uncertain (e.g., Salvadori et al. 2007; Hartwig et al. 2015). It is also possible that the accretion of gas, dust, or even asteroids from the interstellar medium may contaminate the atmosphere of a Pop III star such that it appears to be an extreme Pop II star (e.g., Frebel et al. 2009; Johnson 2015; Komiya et al. 2015, 2016; Shen et al. 2017; Tanaka et al. 2017; Tanikawa et al. 2018). This ambiguity illustrates the importance of methods that do not rely on the abundances of metal-poor stars to evaluate whether or not low-mass Pop III stars exist.

As we will show, the occurrence and properties of low-mass objects around the most metal-poor stars provide a chemical-abundance-independent way to investigate low-mass Pop III star formation. We report the discovery of a low-mass ultra metal-poor (UMP)<sup>2</sup> star in the single-lined spectroscopic binary system 2MASS J18082002–5104378. The secondary in the system, 2MASS J18082002–5104378 B, has a mass  $M_2 = 0.14^{+0.06}_{-0.01} M_\odot$ , near the hydrogen-burning limit for its metallicity. Because of its low mass and metallicity, it has the fewest grams of heavy elements of any known star. We use models of protostellar disks around both UMP and Pop III protostars plus scaling relations for the fragment mass and migration time

<sup>2</sup> Following the definition of Beers & Christlieb (2005), UMP objects have  $-5.0 \lesssim [\text{Fe}/\text{H}] \lesssim -4.0$ .

**Table 1.** Spectroscopic Stellar Parameters for 2MASS J18082002–5104378 A from Meléndez et al. (2016)

Property	Value	Units
Effective temperature $T_{\text{eff}}$	$5440 \pm 100$	K
Surface gravity $\log g$	$3.0 \pm 0.2$	
Microturbulence $v_t$	$1.5 \pm 0.2$	$\text{km s}^{-1}$
Metallicity [Fe/H]	$-4.07 \pm 0.07$	

to argue that the existence of the low-mass UMP star 2MASS J18082002–5104378 B and the extremely metal-poor (EMP)<sup>3</sup> brown dwarf HE 1523–0901 B discovered by Hansen et al. (2015) implies the survival of solar-mass fragments around Pop III stars in the mass range  $10 M_{\odot} \lesssim M_* \lesssim 100 M_{\odot}$ . We describe our observations of the 2MASS J18082002–5104378 system and our data reduction in Section 2. We detail our radial velocity measurement, Keplerian orbital analysis, and Galactic orbit determination of 2MASS J18082002–5104378 and then derive the significance of its existence for Pop III star formation in Section 3. We discuss the overall results and implications in Section 4 and conclude by summarizing our findings in Section 5.

## 2. OBSERVATIONS

The UMP nature of the primary in the 2MASS J18082002–5104378 system was discovered by Meléndez et al. (2016). Those authors measured the spectroscopic stellar parameters we reproduce in Table 1. Meléndez et al. (2016) also noted that 2MASS J18082002–5104378 was a single-lined spectroscopic binary with radial velocity variations in the most luminous component on the order of  $100 \text{ km s}^{-1}$  over a five month period from 2014 October to 2015 March. In addition, Meléndez et al. (2016) found no evidence for a second set of absorption lines in their high-resolution, high signal-to-noise ratio (S/N) spectra. These latter two facts attracted our attention to the 2MASS J18082002–5104378 system, as radial velocity variations of  $100 \text{ km s}^{-1}$  over a five month interval with no evidence for a second set of lines in high-quality high-resolution spectra could only be explained by a neutron star or stellar mass black hole.

We subsequently observed the 2MASS J18082002–5104378 system 14 times between 2016 April and 2017 July with the Magellan Inamori Kyocera Echelle

(MIKE) spectrograph on the Magellan Clay Telescope at Las Campanas Observatory (Bernstein et al. 2003; Shectman & Johns 2003). We used the 0'7 slit and the standard blue and red grating azimuths, yielding spectra between 332 nm and 915 nm with resolution  $R \approx 41,000$  in the blue and  $R \approx 35,000$  in the red. Exposure times between two and five minutes depending on conditions produced spectra that have  $S/N \approx 25 \text{ pixel}^{-1}$  at 400 nm and  $S/N \approx 40 \text{ pixel}^{-1}$  at 460 nm. On each night, we also observed the radial velocity standards HIP 81294 or HIP 90522 from Soubiran et al. (2013). Exposures on both the 2MASS J18082002–5104378 system and the radial velocity standards were followed immediately by ThAr lamp spectra. We collected all other calibration data (e.g., bias, quartz & “milky” flat field, and additional ThAr lamp frames) in the afternoon before each night of observations. We reduced the raw spectra and calibration frames using the CarPy<sup>4</sup> software package (Kelson et al. 2000; Kelson 2003).

In parallel, between 2016 June and 2017 July we collected 31 epochs of low-resolution spectroscopy with the Gemini Multi-Object Spectrograph (GMOS) on the Gemini South telescope (Hook et al. 2004; Gimeno et al. 2016). We used the 0'5 slit and the B600 grating with a central wavelength of 500 nm, producing spectra between 350 and 650 nm with resolution  $R \approx 1,700$ . For each epoch, we collected three individual spectra each with an exposure time 180 s yielding  $S/N \approx 100 \text{ pixel}^{-1}$  at 430 nm. After each science exposure, we obtained CuAr lamp spectra and quartz–tungsten–halogen flat fields. We also observed the radial velocity standard HIP 81294 with the same set-up. We debiased each exposure using its overscan region. We flat fielded and wavelength calibrated each science frame using the quartz–tungsten–halogen and CuAr frames taken immediately following the science exposure. We propagated data quality and inverse variance arrays at every step to obtain at the end a Gaussian extraction of the wavelength-calibrated and transformed image. We continuum normalized each spectrum using a spline function with a mask that excluded strong absorption lines and the gaps between detector chips.

## 3. ANALYSIS

### 3.1. Radial Velocity Measurement

We measured radial velocities from our high-resolution spectra using Tonry & Davis (1979) one-dimensional Fourier cross-correlation as implemented in the FXCOR task available in the Image Reduction and Analysis Fa-

<sup>3</sup> Following the definition of Beers & Christlieb (2005), EMP objects have  $-4.0 \lesssim [\text{Fe}/\text{H}] \lesssim -3.0$ .

<sup>4</sup> <http://code.obs.carnegiescience.edu/mike>

**Table 2.** High-resolution Radial Velocity Observations of 2MASS J18082002-5104378 A

HJD	Radial Velocity	Uncertainty
(d)	(km s <sup>-1</sup> )	(km s <sup>-1</sup> )
VLT/UVES		
2456949.52132	21.19	0.26
2456951.51539	18.15	0.24
2457087.86838	21.94	0.26
Magellan/MIKE		
2457479.88381	8.76	0.62
2457480.90651	7.47	0.40
2457579.66548	13.57	0.54
2457581.73107	10.63	0.32
2457582.64291	10.29	0.50
2457590.69448	9.61	0.32
2457591.59471	10.63	0.36
2457593.53991	13.48	0.40
2457595.46615	16.71	0.92
2457680.48650	19.19	0.66
2457946.72530	21.94	0.28
2457948.57123	24.40	0.28
2457949.59345	25.12	0.26
2457953.78650	25.55	0.32

cility (IRAF; Tody 1986, 1993).<sup>5</sup> After masking out the H- $\gamma$  and H- $\delta$  lines, we cross correlated in the wavelength range 400–460 nm between our observed spectra and a theoretically generated template spectrum from Coelho et al. (2005) interpolated to  $T_{\text{eff}} = 5440$ ,  $\log g = 3.0$ , and  $[\text{Fe}/\text{H}] = -2.45$ . After applying heliocentric corrections, we give our final radial velocity measurements as well as their uncertainties and the Heliocentric Julian Date (HJD) at the start of each observation in Table 2.

We found it impossible to fit a Keplerian orbit to the union of our Magellan/MIKE radial velocities given in Table 2 and the Very Large Telescope (VLT) Ultraviolet and Visual Echelle Spectrograph (UVES; Dekker et al. 2000) radial velocities published in Meléndez et al. (2016). After measuring the radial velocities ourselves for the VLT/UVES spectra described in Meléndez et al. (2016), we found that those authors applied the heliocentric correction to their measured velocities with the wrong sign. Instead of the presence of a neutron star or

stellar mass black hole in the system, it was that mistake that produced the apparent  $100 \text{ km s}^{-1}$  change in the radial velocity of the 2MASS J18082002-5104378 system over a five month interval. We report our own radial velocity measurements based on the Meléndez et al. (2016) VLT/UVES spectra in the first three rows of Table 2. It is clear from Table 2 that the 2MASS J18082002-5104378 system is a single-lined spectroscopic binary, and we describe our Keplerian fit to those data in the following subsection.

We used a two-step procedure to measure radial velocities from our Gemini South/GMOS-S spectra. We first cross-correlated each exposure against a rest-frame continuum-normalized spectrum of the UMP giant CD-38 245. We then corrected each exposure for the measured radial velocity shift and produced a continuum-normalized spectrum of 2MASS J18082002-5104378 using the median flux in each rebinned exposure. We next used the stacked rest-frame spectrum of 2MASS J18082002-5104378 as the template and re-measured the radial velocities of individual exposures by cross-correlation. The radial velocities we report in Table 3 represent the mean heliocentric-corrected radial velocity from three exposures. The listed uncertainty is the standard deviation of three measurements added in quadrature with a systematic uncertainty equal to the mean estimated uncertainty of individual measurements from cross-correlation (about  $5 \text{ km s}^{-1}$ ).

While less precise than the data in Table 2, the data in Table 3 have better time resolution and sufficient radial velocity precision to recover any large-amplitude radial velocity variations if present. We did not observe any large-amplitude radial velocity variations over a 13 month period, supporting our analysis in the preceding paragraph. We experimented with fitting the data in Table 2 alone and in concert with the data in Table 3. We found that the resulting Keplerian orbital elements were consistent between the two cases but less precise in the latter case. Consequently, we did not use the data in Table 3 in our final Keplerian fit described in the next subsection.

### 3.2. Keplerian Orbit Parameter Estimation

We fit a Keplerian orbit to the radial velocities in Table 2 using the Bayesian Markov chain Monte Carlo (MCMC) code ExoFit<sup>6</sup> (Balan & Lahav 2009). We used the default ExoFit parameters with one exception: we initialized the starting point of the MCMC at  $e = 0.1$  instead of  $e = 0.5$ . We plot the fitted Keplerian orbit with the radial velocities from Tables 2 and 3 in Figures 1

<sup>5</sup> IRAF is distributed by the National Optical Astronomy Observatories, which are operated by the Association of Universities for Research in Astronomy, Inc., under cooperative agreement with the National Science Foundation.

<sup>6</sup> <http://www.homepages.ucl.ac.uk/~ucapola/exofit.html>

**Table 3.** Gemini South/GMOS-S Low-resolution Radial Velocity Observations of 2MASS J18082002-5104378 A

HJD	Radial Velocity	Uncertainty
(d)	(km s <sup>-1</sup> )	(km s <sup>-1</sup> )
2457559.08034	8.5	5.7
2457563.32367	20.9	5.3
2457584.09253	-6.0	5.7
2457590.06602	6.3	5.5
2457603.99236	26.3	6.2
2457634.97860	23.0	5.1
2457654.00692	7.4	5.1
2457663.99389	15.7	5.1
2457681.01178	21.1	5.6
2457683.07641	5.2	5.6
2457686.02310	14.9	5.1
2457808.38897	26.4	5.8
2457815.36205	21.0	5.2
2457836.37176	13.4	5.1
2457842.32615	23.9	5.2
2457850.41464	32.2	5.2
2457869.34934	10.0	5.0
2457872.35197	21.2	5.1
2457883.17645	22.3	5.2
2457890.38603	16.0	5.7
2457901.30690	4.6	5.8
2457923.23911	28.2	5.2
2457934.12196	9.0	5.3
2457944.10230	20.2	5.3
2457948.03707	28.7	6.3
2457954.20577	20.9	6.6
2457955.20855	31.1	5.3
2457956.08313	23.1	5.3
2457957.31008	18.0	5.3
2457958.06814	19.8	5.3
2457961.03876	19.4	5.6

and 2. We include a corner plot illustrating the covariances of the fitted parameters in Figure 3. We found an orbital period  $P = 34.757 \pm 0.010$  days, a system velocity  $\gamma = 16.54 \pm 0.12$  km s<sup>-1</sup>, a velocity semi-amplitude  $K = 9.2 \pm 0.2$  km s<sup>-1</sup>, an eccentricity  $e = 0.02^{+0.02}_{-0.01}$ , a longitude of periastron  $\omega = 291^{+22}_{-32}$  deg, and a time of periastron  $t_0 = 2456945.9^{+2.1}_{-3.1}$  HJD. We also calculated the projected semimajor axis  $a_1 \sin i$  as

$$a_1 \sin i = \frac{PK(1-e^2)^{1/2}}{2\pi} = 6.3 \pm 0.1 R_\odot, \quad (1)$$

and the mass function  $f(M)$  as

$$f(M) = \frac{PK^3(1-e^2)^{3/2}}{2\pi G} = 0.0028 \pm 0.0001 M_\odot. \quad (2)$$

We summarize the properties of the 2MASS J18082002-5104378 system in Table 4.<sup>7</sup>

The mass function given above indicates that the visible star is the primary in the system which we now denote 2MASS J18082002-5104378 A. To estimate the properties of the unseen component 2MASS J18082002-5104378 B, we first used the `isochrones`<sup>8</sup> (Morton 2015) package to estimate the mass of the visible star 2MASS J18082002-5104378 A using as inputs its:

1. estimated spectroscopic parameters and associated uncertainties from Meléndez et al. (2016);
2.  $u$ ,  $v$ ,  $g$ , and  $r$  magnitudes and associated uncertainties from Data Release (DR) 1.1 of the SkyMapper Southern Sky Survey (Wolf et al. 2018);
3.  $J$ ,  $H$ , and  $K_s$  magnitudes and associated uncertainties from the 2MASS All-sky Point Source Catalog (Skrutskie et al. 2006);
4.  $W1$ ,  $W2$ , and  $W3$  magnitudes and associated uncertainties from the AllWISE Source Catalog (Wright et al. 2010; Mainzer et al. 2011);
5. *Gaia* DR2 parallax and uncertainty (Gaia Collaboration et al. 2016, 2018; Arenou et al. 2018; Hambly et al. 2018; Lindegren et al. 2018; Luri et al. 2018).

We used `isochrones` to fit the Dartmouth Stellar Evolution Database (Dotter et al. 2007, 2008) library generated with the Dartmouth Stellar Evolution Program (DSEP) to these observables using `MultiNest`<sup>9</sup> (Feroz

<sup>7</sup> Though we did not use the available *Gaia* DR2 (Salgado et al. 2017; Evans et al. 2018; Riello et al. 2018) or APASS photometry (Henden et al. 2016) for 2MASS J18082002-5104378, we provide those data in Table 4 for context.

<sup>8</sup> <https://github.com/timothydmorton/isochrones>

<sup>9</sup> <https://ccpforge.cse.rl.ac.uk/gf/project/multinest/>

**Table 4.** 2MASS J18082002–5104378 System Properties

Property	Value	Units
Observed Properties		
Gaia DR2 R.A. $\alpha$ (J2000)	18 08 20.0314	h m s
Gaia DR2 decl. $\delta$ (J2000)	-51 04 37.884	d m s
Gaia DR2 galactic longitude $l$ (J2000)	342.5353	degrees
Gaia DR2 galactic latitude $b$ (J2000)	-14.4898	degrees
Gaia DR2 proper motion $\mu_\alpha \cos \delta$	$-5.63 \pm 0.07$	mas yr <sup>-1</sup>
Gaia DR2 proper motion $\mu_\delta$	$-12.64 \pm 0.06$	mas yr <sup>-1</sup>
Gaia DR2 parallax $\pi$	$1.64 \pm 0.04$	mas
Gaia DR2 $G$	$11.7562 \pm 0.0003$	Vega mag
Gaia DR2 $G_{BP}$	$12.119 \pm 0.002$	Vega mag
Gaia DR2 $G_{RP}$	$11.215 \pm 0.002$	Vega mag
APASS $B$	$12.546 \pm 0.018$	Vega mag
APASS $V$	$11.930 \pm 0.031$	Vega mag
APASS $g'$	$12.219 \pm 0.014$	AB mag
APASS $r'$	$11.736 \pm 0.019$	AB mag
APASS $i'$	$11.625 \pm 0.017$	AB mag
SkyMapper $u$	$13.331 \pm 0.005$	AB mag
SkyMapper $v$	$12.892 \pm 0.002$	AB mag
SkyMapper $g$	$12.067 \pm 0.002$	AB mag
SkyMapper $r$	$11.747 \pm 0.002$	AB mag
2MASS $J$	$10.527 \pm 0.026$	Vega mag
2MASS $H$	$10.158 \pm 0.026$	Vega mag
2MASS $K_s$	$10.088 \pm 0.026$	Vega mag
WISE $W1$	$9.992 \pm 0.023$	Vega mag
WISE $W2$	$9.997 \pm 0.020$	Vega mag
WISE $W3$	$9.919 \pm 0.054$	Vega mag
Orbital period $P$	$34.757 \pm 0.010$	day
System velocity $\gamma$	$16.54 \pm 0.12$	km s <sup>-1</sup>
Velocity semi-amplitude $K$	$9.2 \pm 0.2$	km s <sup>-1</sup>
Eccentricity $e$	$0.02^{+0.02}_{-0.01}$	
Longitude of periastron $\omega$	$291^{+22}_{-32}$	deg
Time of periastron $t_0$	$2456945.9^{+2.1}_{-3.1}$	HJD
Projected semimajor axis $a_1 \sin i$	$6.3 \pm 0.1$	$R_\odot$
Mass function $f(M)$	$0.0028 \pm 0.0001$	$M_\odot$
Time span	$28.894 \pm 0.008$	periods
Inferred Properties		
Primary mass $M_1$	$0.7599 \pm 0.0001$	$M_\odot$
System age $\tau$	$13.53 \pm 0.002$	Gyr
Minimum secondary mass $M_{2,\min}$	$0.131 \pm 0.002$	$M_\odot$
Secondary mass $M_2$	$0.14^{+0.06}_{-0.01}$	$M_\odot$
Semimajor axis $a$	$0.202^{+0.004}_{-0.001}$	au
Total Galactic velocity $v$	$207.5^{+1.1}_{-1.2}$	km s <sup>-1</sup>
Pericenter of Galactic orbit $R_{\text{peri}}$	$5.56 \pm 0.07$	kpc
Apocenter of Galactic orbit $R_{\text{apo}}$	$7.66 \pm 0.02$	kpc
Eccentricity of Galactic orbit $e_G$	$0.158^{+0.005}_{-0.004}$	
Maximum distance from Galactic plane $z_{\text{max}}$	$0.126^{+0.005}_{-0.003}$	kpc

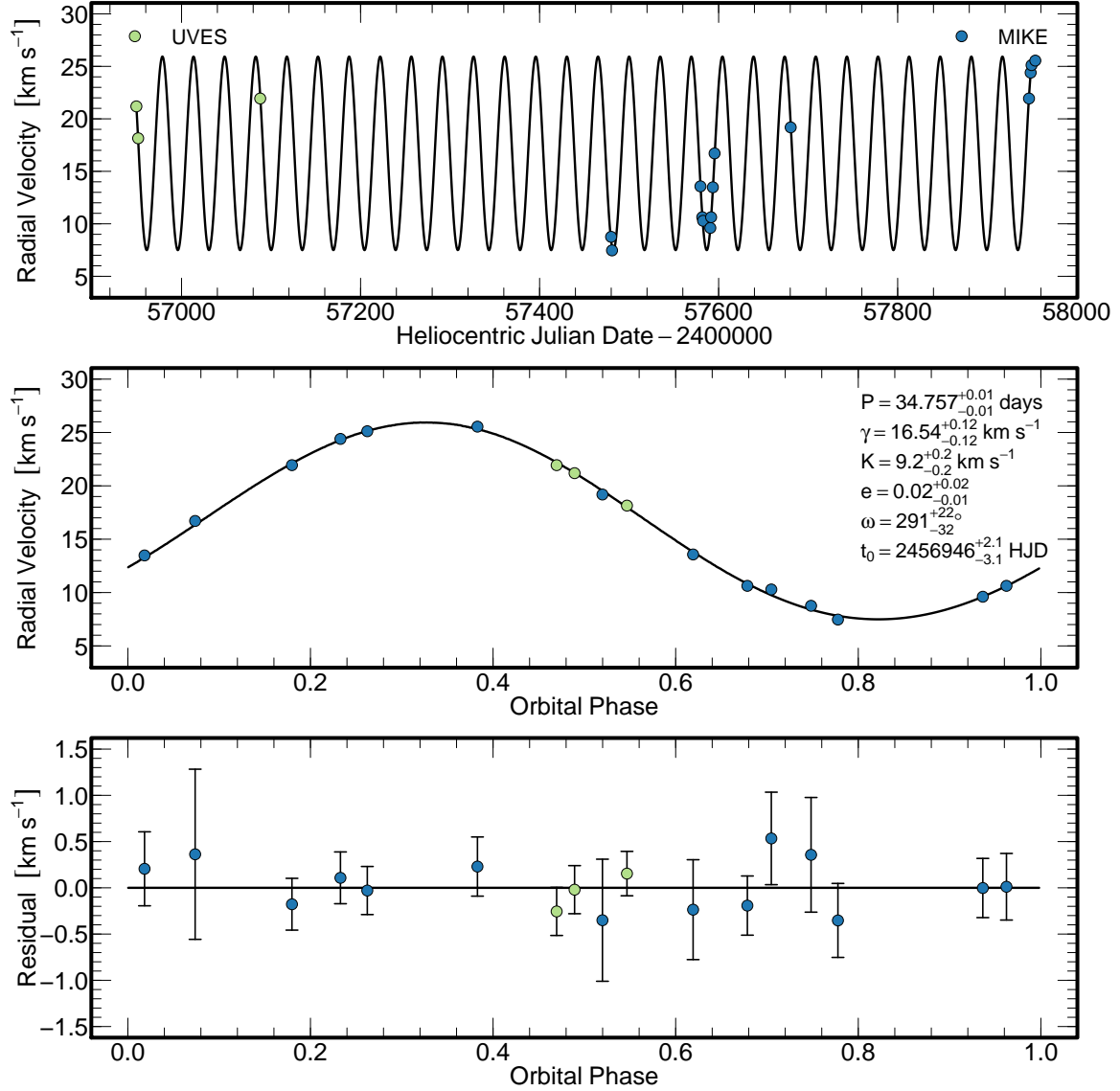


**Figure 1.** Keplerian orbit of 2MASS J18082002-5104378 system alongside radial velocities measured with VLT/UVES and Magellan/MIKE. The points are the individual radial velocities from Table 2, while the curve is the orbit resulting from a Keplerian fit to those data. We plot the radial velocity uncertainties in each panel, but they are smaller than the plotted points in the top two panels.

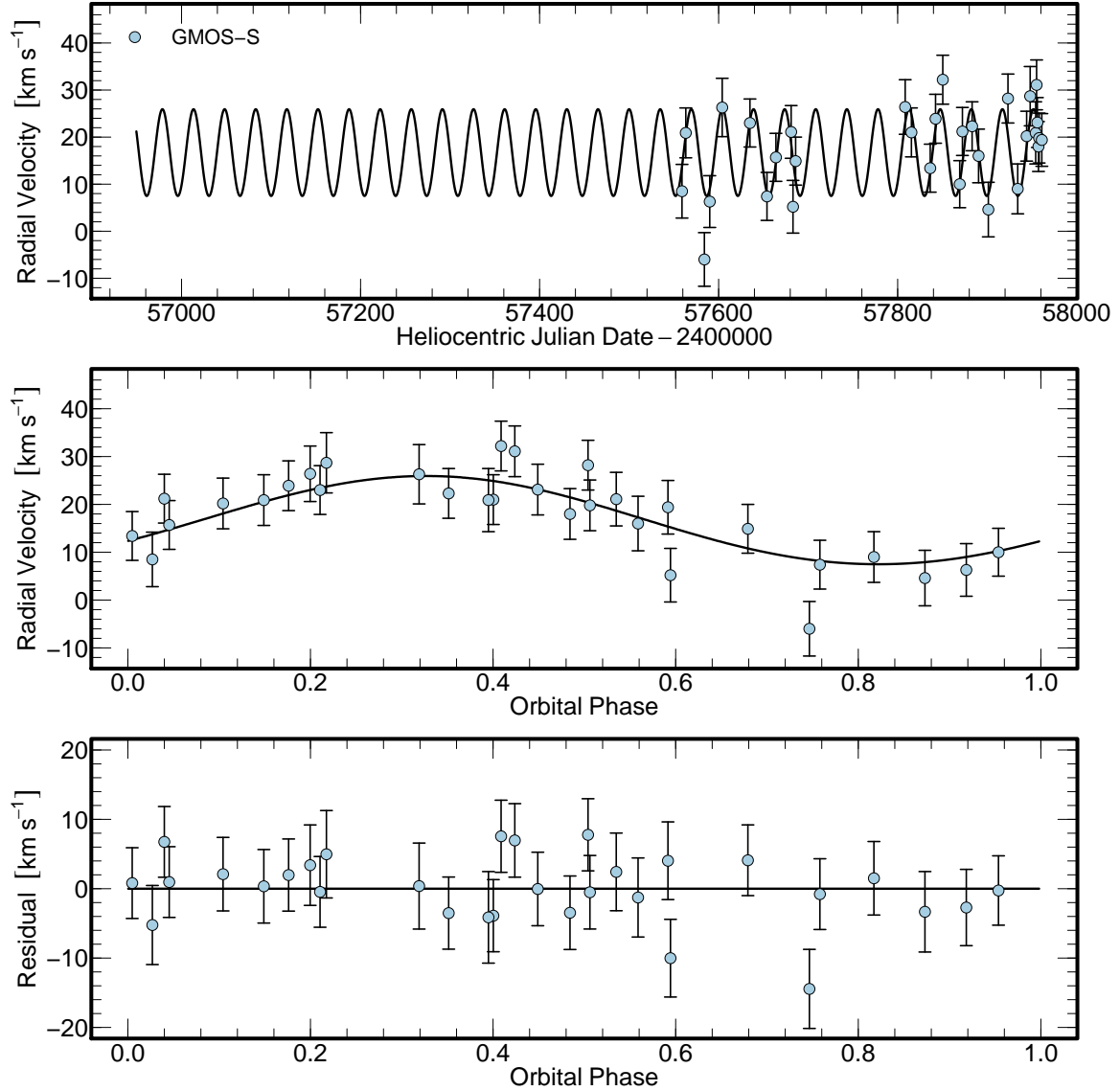


**Figure 2.** Keplerian orbit of 2MASS J18082002–5104378 system alongside radial velocities measured with Gemini South/GMOS-S. The points are the individual radial velocities from Table 3, while the curve is the orbit resulting from a Keplerian fit to data in Table 2.

& Hobson 2008; Feroz et al. 2009, 2013). We restricted the Dartmouth library to  $\alpha$ -enhanced composition  $[\alpha/\text{Fe}] = +0.4$ , stellar age  $\tau$  in the range  $10.0 \text{ Gyr} \leq \tau \leq 13.721 \text{ Gyr}$ , and extinction  $A_V$  in the range  $0 \text{ mag} \leq A_V \leq 1.0 \text{ mag}$ . We limited distances  $d$  considered to the range  $561.7978 \text{ pc} \leq d \leq 632.9114 \text{ pc}$  (the  $2\text{-}\sigma$  range for the system from *Gaia* DR2). Given these constraints, we found that the primary 2MASS J18082002–5104378 A has a mass  $M_1 = 0.7599 \pm 0.0001 M_\odot$  and an age  $\tau = 13.535 \pm 0.002 \text{ Gyr}$ . We summarize our preferred isochrone-derived parameters for 2MASS J18082002–5104378 A in Table 5.

The Dartmouth isochrones prefer a slightly warmer and more metal-rich star than suggested by Meléndez

et al. (2016). The estimated effective temperature is degenerate with extinction, however, and that degeneracy may explain the slightly higher metallicity suggested by the isochrone analysis. It is also possible that 2MASS J18082002–5104378 A is slightly carbon enhanced, as the Meléndez et al. (2016) upper limit on the carbon abundance  $[\text{C}/\text{Fe}]$  is  $[\text{C}/\text{Fe}] \lesssim +0.5$ . If 2MASS J18082002–5104378 A has  $[\text{C}/\text{Fe}] \approx +0.5$ , then that would increase its total metallicity  $[\text{M}/\text{H}]$  to  $[\text{M}/\text{H}] \approx -3.50$  in accord with the isochrone estimate.

To investigate the possibility of systematic error resulting from our use of the Dartmouth library, we also estimated the mass and age of 2MASS J18082002–5104378 A using two additional isochrone libraries. We



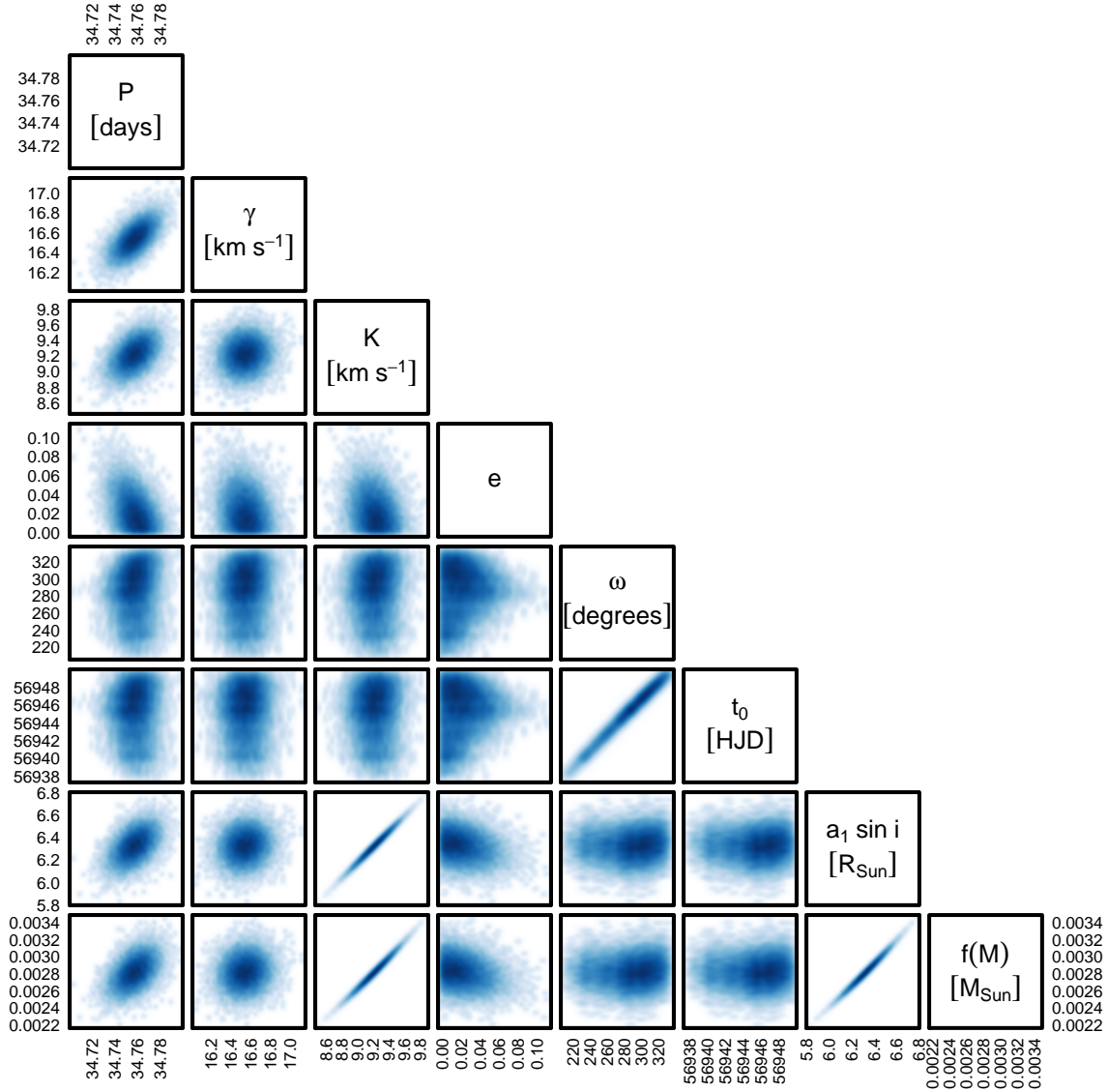


**Figure 3.** Corner plot resulting from our MCMC fit of a Keplerian orbit to the radial velocities of the 2MASS J18082002–5104378 system given in Table 2. We found an orbital period  $P = 34.757 \pm 0.010$  days, a system velocity  $\gamma = 16.54 \pm 0.12$  km s<sup>-1</sup>, a velocity semi-amplitude  $K = 9.2 \pm 0.2$  km s<sup>-1</sup>, an eccentricity  $e = 0.02^{+0.02}_{-0.01}$ , a longitude of periastron  $\omega = 291^{+22}_{-32}$  deg, and a time of periastron  $t_0 = 2456945.9^{+2.1}_{-3.1}$  HJD.

**Table 5.** Isochrone-derived Stellar Parameters for 2MASS J18082002–5104378 A

Property	Value	Units
Effective temperature $T_{\text{eff}}$	$5871^{+17}_{-18}$	K
Surface gravity $\log g$	$3.378^{+0.007}_{-0.006}$	
Metallicity [Fe/H]	$-3.50 \pm 0.02$	
Extinction $A_V$	$0.40 \pm 0.01$	mag
Mass $M_*$	$0.7599 \pm 0.0001$	$M_{\odot}$
System age $\tau$	$13.535 \pm 0.002$	Gyr

first used **isochrones** to fit the MESA Isochrones & Stellar Tracks (MIST; Choi et al. 2016; Dotter 2016) library generated with the Modules for Experiments in Stellar Astrophysics (MESA; Paxton et al. 2011, 2013, 2015) code to these observables using **MultiNest**. We found  $M_1 = 0.80728^{+0.00004}_{-0.00005} M_{\odot}$  and  $\tau = 11.12 \pm 0.07$  Gyr. We then used the PARAM 1.3 web interface for the Bayesian estimation of stellar parameters<sup>10</sup> (da Silva et al. 2006). We found  $M_1 = 0.768 \pm 0.011 M_{\odot}$  and  $\tau = 12.747 \pm 0.553$  Gyr. We prefer the mass and age pro-

<sup>10</sup> <http://stev.oapd.inaf.it/cgi-bin/param.1.3>

duced by the Dartmouth grid because it accounts for the  $\alpha$ -enhanced composition of 2MASS J18082002–5104378 A and because its estimate has a higher log-likelihood than either the MIST or PARAM 1.3 estimates.

To estimate the mass of 2MASS J18082002–5104378 B, we solved the nonlinear mass function equation

$$\frac{M_1 \sin^3 i}{f(m)} q^3 - (1 + q)^2 = 0, \quad (3)$$

where  $q = M_2/M_1$  and the mass function  $f(m)$  is defined as

$$f(m) = \frac{M_2^3 \sin^3 i}{(M_1 + M_2)^2} = \frac{PK^3 (1 - e^2)^{3/2}}{2\pi G}. \quad (4)$$

We used the distribution of  $\sin^3 i$  proposed by Hogeveen (1992). Generalizing the method put forward by Halbwachs (1987), Hogeveen showed that the assumption  $P(i) di = (4/\pi) \sin^2 i di$  produces better estimates of the measured mass ratios of double-lined spectroscopic binaries than the standard assumption of random inclinations  $P(i) di = \sin i di$ . This bias toward edge-on systems arises because  $K$ -limited searches for spectroscopic binaries will tend to discover systems with orbital inclinations closer to  $i = 90^\circ$  than to  $i = 0^\circ$ . Under the Hogeveen (1992) assumption, the distribution of  $x = \sin^3 i$  becomes

$$P(x) dx = \frac{4}{3\pi} \left(1 - x^{2/3}\right)^{-1/2} dx. \quad (5)$$

We found a mass  $M_2 = 0.14^{+0.06}_{-0.01} M_\odot$  and a minimum mass  $M_{2,\min} = 0.131 \pm 0.002 M_\odot$  (assuming  $\sin^3 i = 1$ ). If we instead assume a single average value for  $\langle \sin^3 i \rangle = 0.679$  in place of averaging over the entire distribution of  $\sin^3 i$ , we find  $M_2 = 0.151 \pm 0.003 M_\odot$ . This inferred mass makes 2MASS J18082002–5104378 B the lowest-mass UMP star known. Indeed, it is near the hydrogen-burning limit at  $M_* \approx 0.092 M_\odot$  for a star of its composition (Saumon et al. 1994). We provide a corner plot illustrating the covariances of the parameters necessary for the mass calculation in Figure 4.

We calculated an upper limit on the mass of 2MASS J18082002–5104378 B based on the lack of a second peak in our cross-correlation analysis. The UVES data we analyzed have  $S/N \approx 50 \text{ pixel}^{-1}$  between 400 and 460 nm, so a secondary star with a similar spectrum to 2MASS J18082002–5104378 A that is less than three magnitudes fainter in the  $B$  band would be detectable. Using a MIST isochrone with the same age we calculated for 2MASS J18082002–5104378 A, that corresponds to an upper limit on the secondary mass  $M_{2,\max} \approx 0.6 M_\odot$ .

### 3.3. Galactic Orbit Estimation

To better understand the origin of the 2MASS J18082002–5104378 system, we calculated its Galactic orbit using `galpy`<sup>11</sup>. We sampled 1000 Monte Carlo realizations from the *Gaia* DR2 astrometric solution for 2MASS J18082002–5104378 taking full account of the covariances between position, parallax, and proper motion. We used our posterior on the system radial velocity  $\gamma$  and assumed no covariance between our measured radial velocity and the *Gaia* DR2 astrometric solution. We used each Monte Carlo realization as an initial condition for an orbit and integrated it forward 10 Gyr in a Milky Way-like potential. We adopted the `MWPotential2014` described by Bovy (2015). In that model, the bulge is parameterized as a power-law density profile that is exponentially cut-off at 1.9 kpc with a power-law exponent of  $-1.8$ . The disk is represented by a Miyamoto–Nagai potential with a radial scale length of 3 kpc and a vertical scale height of 280 pc (Miyamoto & Nagai 1975). The halo is modeled as a Navarro–Frenk–White halo with a scale length of 16 kpc (Navarro et al. 1996). We set the solar distance to the Galactic center to  $R_0 = 8.122$  kpc, the circular velocity at the Sun to  $V_0 = 238 \text{ km s}^{-1}$ , the height of the Sun above the plane to  $z_0 = 25$  pc, and the solar motion with the respect to the local standard of rest to  $(U_\odot, V_\odot, W_\odot) = (10.0, 11.0, 7.0) \text{ km s}^{-1}$  (Jurić et al. 2008; Bland-Hawthorn & Gerhard 2016; Gravity Collaboration et al. 2018).

We found that the 2MASS J18082002–5104378 system is on a thin disk like orbit through the Galaxy with pericenter  $R_{\text{peri}} = 5.56 \pm 0.07$  kpc, apocenter  $R_{\text{apo}} = 7.66 \pm 0.02$  kpc, Galactic eccentricity  $e_G = 0.158^{+0.005}_{-0.004}$ , and maximum distance from Galactic plane  $z_{\text{max}} = 0.126^{+0.005}_{-0.003}$  kpc. By some margin, the 2MASS J18082002–5104378 system is the most metal-poor star system on a thin disk orbit (e.g., Casagrande et al. 2011; Bensby et al. 2014; Beers et al. 2017).

### 3.4. Importance for Pop III Star Formation

To evaluate the implications for Pop III stars of our discovery of the low-mass UMP star 2MASS J18082002–5104378 B, we explored the properties and survival of fragments in models of UMP and primordial composition protostellar disks published in Tanaka & Omukai (2014). A Keplerian disk can be expected to fragment if its Toomre parameter  $Q$  is

$$Q = \frac{\Omega c_s}{\pi G \Sigma} \lesssim 1, \quad (6)$$

<sup>11</sup> <https://github.com/jobovy/galpy>

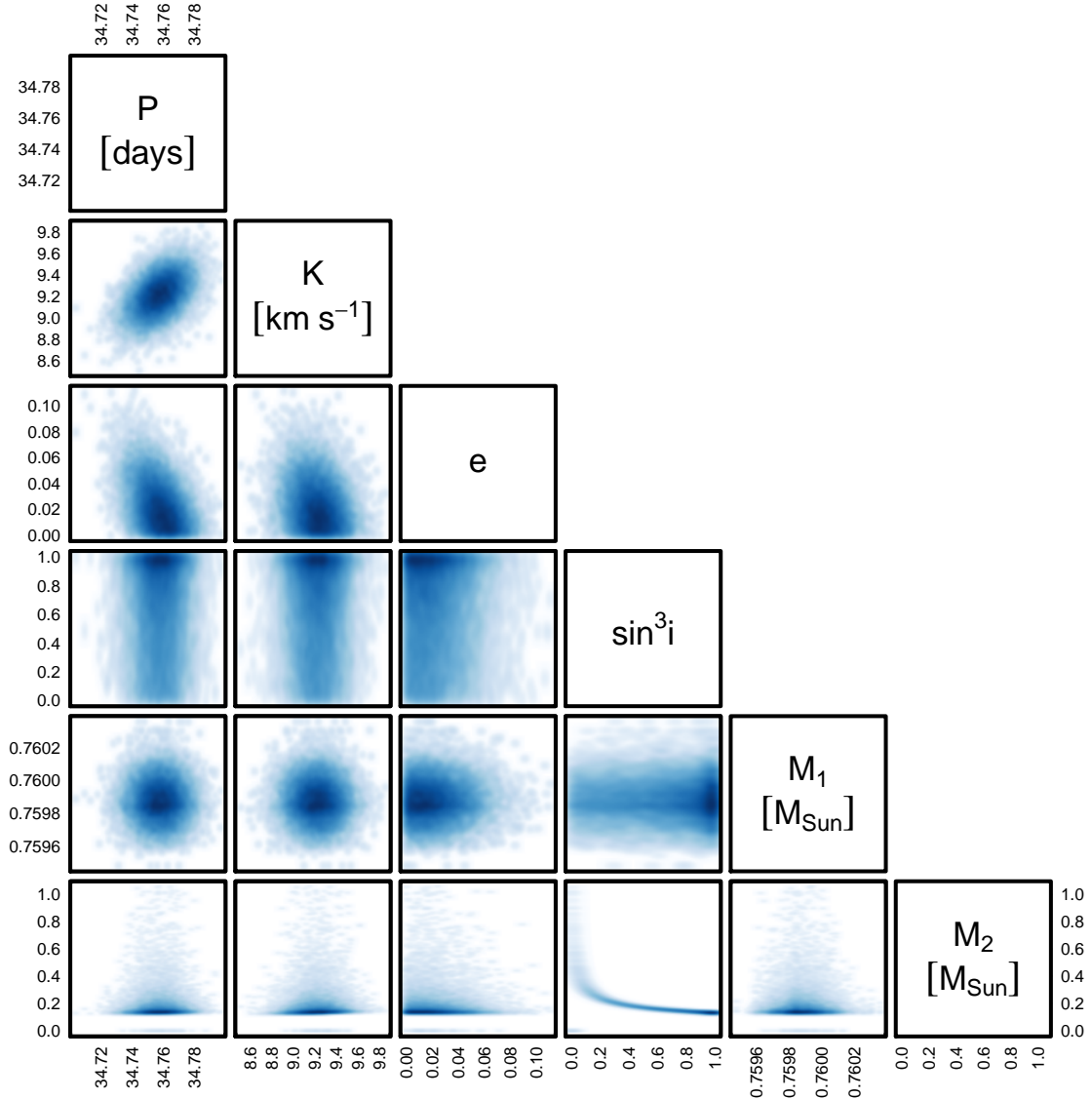


**Figure 4.** Corner plot for our estimate of the mass of the secondary in the 2MASS J18082002–5104378 system. The posteriors on  $P$ ,  $K$ , and  $e$  came from our MCMC fit of a Keplerian orbit to the radial velocities in Table 2. The distribution of  $\sin^3 i$  is from Hogeveen (1992). The posterior on the mass of the primary  $M_1$  came from our isochrone analysis. The mass of the secondary  $M_2$  came from solving the nonlinear mass function equation. We found that the mass of the secondary 2MASS J18082002–5104378 B is  $M_2 = 0.14^{+0.06}_{-0.01} M_\odot$ , making it the lowest-mass UMP star known and placing it near the hydrogen-burning limit at  $M_* \approx 0.092 M_\odot$  for a star of its composition (Saumon et al. 1994).

where  $\Omega$  is the Keplerian orbital frequency,  $c_s$  is the gas sound speed, and  $\Sigma$  is the gas surface density.  $\Omega$ ,  $c_s$ , and  $\Sigma$  are all implicit functions of the radial coordinate  $r$ . In this situation, the typical fragment mass scale is

$$M_{\text{frag}} \sim \Sigma H^2, \quad (7)$$

where  $H = c_s/\Omega$  is the characteristic disk thickness (e.g., Paardekooper & Johansen 2018). A scaling relation for the mass of the typical fragment that will form in an unstable disk is therefore

$$\frac{M_{\text{frag},2}}{M_{\text{frag},1}} = \left( \frac{\Sigma_2}{\Sigma_1} \right) \left( \frac{H_2}{H_1} \right)^2. \quad (8)$$

Once formed, a fragment in a nonaxisymmetric protostellar disk will lose orbital energy and angular momentum due to gravitational torques between the fragment and the disk. As shown by Baruteau et al. (2011), fragments formed via gravitational instability will not be massive enough relative to the local disk mass to significantly perturb the disk structure. Assuming the frag-

ment moves on a circular orbit at the local Keplerian frequency, the characteristic fragment migration time is given by

$$t_{\text{mig}} = \frac{h^2}{q} \frac{M_*}{r^2 \Sigma} \Omega^{-1}, \quad (9)$$

where  $h = H/r$  is the disk aspect ratio and  $q = M_{\text{frag}}/M_*$  is ratio between the fragment mass and stellar mass (e.g., Paardekooper & Johansen 2018). A scaling relation for the typical fragment migration time in an unstable disk is therefore

$$\frac{t_{\text{mig},2}}{t_{\text{mig},1}} = \left(\frac{h_2}{h_1}\right)^2 \left(\frac{q_1}{q_2}\right) \left(\frac{M_{*,2}}{M_{*,1}}\right) \left(\frac{r_1}{r_2}\right)^2 \left(\frac{\Sigma_1}{\Sigma_2}\right) \left(\frac{\Omega_1}{\Omega_2}\right). \quad (10)$$

To calculate the disk properties necessary to use the scaling relations given by Equations (8) and (10), we used the Tanaka & Omukai (2014) models and assumed a mean molecular weight  $\mu = 2.29$  for the fully molecular gas expected at protostellar disk densities (e.g., Schneider et al. 2012). We report all values necessary to use Equations (8) and (10) in Table 6.

Because it is so tightly bound to J18082002–5104378 A, 2MASS J18082002–5104378 B is extraordinarily unlikely to have been gravitationally captured outside of the birth environment of the former. They must therefore have formed in the same molecular core and thus have the same composition. It is reasonable to assume that the short-period, low-mass star 2MASS J18082002–5104378 B formed via disk fragmentation and arrived close to its host star because of disk migration (e.g., Kratter & Lodato 2016). In that case, its formation and survival at  $M_* \approx 0.14 M_\odot$  in an UMP protostellar disk with  $[\text{Fe}/\text{H}] \approx -4.1$  around the  $M_* \approx 0.76 M_\odot$  star 2MASS J18082002–5104378 A can be used with Equations (8) and (10) plus the data from Tanaka & Omukai (2014) in Table 6 to explore the fragmentation mass scale and migration times in primordial composition protostellar disks around Pop III stars.

According to Tanaka & Omukai (2014), a protostellar disk around a  $M_* = 1.0 M_\odot$  UMP star at  $r = 10^{0.50}$  au is marginally stable (i.e.,  $Q \approx 1$ ). At  $r \gtrsim 10^{1.0}$  au, that same disk is gravitationally unstable (i.e.,  $Q < 1$ ). We found that for a  $M_* = 10 M_\odot$  Pop III star, Equation (8) implies  $M_{\text{frag}} \approx (0.25, 0.88) M_\odot$  at  $r = (10^{0.5}, 10^{1.0})$  au. Let  $t_{\text{mig},1}$  be defined as the migration time of a fragment in an UMP protostellar disk with the same mass as 2MASS J18082002–5104378 B. For that fragment at  $r = (10^{0.5}, 10^{1.0})$  au, Equation (10) indicates

a migration time  $t_{\text{mig},2} \approx (1.7, 1.4) t_{\text{mig},1}$ . For a  $M_* = 100 M_\odot$  Pop III star, the expected fragment mass is  $M_{\text{frag}} \approx (1.0, 0.25) M_\odot$  and  $t_{\text{mig},2} \approx (22, 3.5) t_{\text{mig},1}$  at  $r = (10^{0.5}, 10^1)$  au. In words, scaling from the 2MASS J18082002–5104378 system yields fragments in the Pop III disk with  $M_{\text{frag}} \lesssim 1.0 M_\odot$  and  $t_{\text{mig},2} \gtrsim t_{\text{mig},1}$ .

We note that Tanaka & Omukai (2014) were forced to assume a Shakura & Sunyaev (1973)  $\alpha$  parameter to account for the efficiency of angular momentum transport in their disk model. In a disk with  $Q \sim 1$ , the angular momentum transport parameterized by  $\alpha$  is dominated by torques due to spiral arms arising because the disk is near gravitational instability. In this context, the contribution from these spiral arms parameterized by  $\alpha_{\text{GI,max}}$  dominates the total angular momentum transport compared to other sources like the magnetorotational instability. While primordial composition disks in the fiducial model of Tanaka & Omukai (2014) with  $\alpha_{\text{GI,max}} = 1$  will have  $Q \approx 1.3$  at  $a = (10^{0.5}, 10^{1.0})$  au and therefore be formally stable against fragmentation, they admit that lower values of  $\alpha_{\text{GI,max}} = 0.07$  are equally plausible. A smaller  $\alpha_{\text{GI,max}}$  would make a disk less able to transport angular momentum and more likely to fragment. Indeed, when  $Q \sim 1$  Equation (15) of Tanaka & Omukai (2014) shows that  $Q$  is linearly proportional to  $\alpha_{\text{GI,max}}$ . Since the Tanaka & Omukai (2014) UMP and primordial composition disks have  $Q \approx 1.3$  when  $\alpha_{\text{GI,max}} = 1$ , even a slightly smaller  $\alpha_{\text{GI,max}} \approx 0.8$  would cause  $Q$  to dip below 1 and therefore cause disk fragmentation. For these reasons, we assert that it is reasonable to consider the possibility that both primordial composition and UMP disks will fragment at  $a = (10^{0.5}, 10^{1.0})$  au.

Hansen et al. (2015) discovered an even lower mass companion in the EMP single-lined spectroscopic binary system HE 1523–0901. That system has Keplerian orbital parameters  $P = 303.05 \pm 0.25$  day,  $K = 0.350 \pm 0.003$  km s<sup>−1</sup>, and  $e = 0.163 \pm 0.010$ . We calculated the mass of the primary in the system—HE 1523–0901 A—as described in Section 3.2. We found that it has  $M_* = 0.83 \pm 0.01 M_\odot$ . The system’s Keplerian parameters and primary mass imply that the secondary in the system—HE 1523–0901 B—has  $M_2 = 0.011^{+0.003}_{-0.001} M_\odot = 11^{+4}_{-1} M_{\text{Jup}}$ .

At the edge of a protostellar disk where it is most unstable and fragmentation is most likely, the properties of HE 1523–0901 B imply fragmentation and fragment survival in both primordial composition disks around the  $M_* = 10 M_\odot$  and  $M_* = 100 M_\odot$  Pop III stars considered above. Let  $t_{\text{mig},1}$  be defined as the migration time of a fragment in an UMP protostellar disk with the same mass as HE 1523–0901 B starting from the edge of that disk at  $r = 10^{1.5}$  au. For the edge of the disk

**Table 6.** Protostellar Disk Properties from Tanaka & Omukai (2014)

Composition	$M_*$	$r$	$T$	$\rho$	$c_s$	$\Omega$	$H$	$\Sigma$
	( $M_\odot$ )	(au)	(K)	( $\text{g cm}^{-3}$ )	( $\text{cm s}^{-1}$ )	( $\text{s}^{-1}$ )	(au)	( $\text{g cm}^{-2}$ )
$Z = 10^{-4} Z_\odot$	1	$10^{0.5}$	$5.0 \times 10^2$	$1.7 \times 10^{-9}$	$1.3 \times 10^5$	$3.5 \times 10^{-8}$	0.25	$6.3 \times 10^3$
	1	$10^{1.0}$	$2.0 \times 10^2$	$8.4 \times 10^{-11}$	$8.5 \times 10^4$	$6.3 \times 10^{-9}$	0.90	$1.1 \times 10^3$
	1	$10^{1.5a}$	$1.0 \times 10^2$	$6.7 \times 10^{-12}$	$6.0 \times 10^4$	$1.1 \times 10^{-9}$	3.6	$3.6 \times 10^2$
$Z = 0$	10	$10^{0.5}$	$1.6 \times 10^3$	$1.7 \times 10^{-8}$	$2.4 \times 10^5$	$1.1 \times 10^{-7}$	0.14	$3.6 \times 10^4$
	10	$10^{1.0}$	$2.0 \times 10^3$	$5.3 \times 10^{-10}$	$2.7 \times 10^5$	$2.0 \times 10^{-8}$	0.90	$7.1 \times 10^3$
	10	$10^{2.1a}$	$7.9 \times 10^2$	$3.3 \times 10^{-13}$	$1.7 \times 10^5$	$4.5 \times 10^{-10}$	25	$1.3 \times 10^2$
$Z = 0$	100	$10^{0.5}$	$4.0 \times 10^4$	$1.7 \times 10^{-8}$	$1.2 \times 10^6$	$3.5 \times 10^{-7}$	0.23	$5.7 \times 10^4$
	100	$10^{1.0}$	$1.6 \times 10^3$	$6.7 \times 10^{-9}$	$2.4 \times 10^5$	$6.3 \times 10^{-8}$	0.25	$2.5 \times 10^4$
	100	$10^{3.2a}$	$3.2 \times 10^2$	$4.2 \times 10^{-15}$	$1.1 \times 10^5$	$3.2 \times 10^{-11}$	230	$1.4 \times 10^1$

<sup>a</sup>Outer edge of disk

around the  $M_* = 10 M_\odot$  star at  $r = 10^{2.1}$  au, we found  $M_{\text{frag}} \approx 0.18 M_\odot$  and  $t_{\text{mig},2} \approx 12 t_{\text{mig},1}$ . For the edge of the disk around the  $M_* = 100 M_\odot$  star at  $r = 10^{3.2}$  au, we found  $M_{\text{frag}} \approx 1.6 M_\odot$  and  $t_{\text{mig},2} \approx 52 t_{\text{mig},1}$ . Once again, scaling from the HE 1523–0901 system yields fragments in the Pop III disk with  $M_{\text{frag}} \sim 1.0 M_\odot$  and  $t_{\text{mig},2} \gtrsim t_{\text{mig},1}$ . These calculations collectively support the idea that solar-mass fragments can form in primordial composition disks around Pop III stars in the mass range  $10 M_\odot \lesssim M_* \lesssim 100 M_\odot$  and subsequently survive disk migration without merging with the primary forming at the center of the disk.

It is important to note several caveats to our inferences based on the existence of 2MASS J18082002–5104378 B and HE 1523–0901 B. If the 2MASS J18082002–5104378 and HE 1523–0901 systems formed via fragmentation at the filament or molecular core scales (e.g., Turk et al. 2009; Chiaki et al. 2016), then the scaling relation argument presented above would not apply. Our study relies on the fidelity of the Tanaka & Omukai (2014) disk models, so any unaccounted-for physics in those models will affect our analysis. For example, it is possible that the transport of angular momentum in UMP and primordial composition disks differs in a way that was not accounted for by Tanaka & Omukai (2014). If that is so, then our scaling relation analysis will be affected. While our scaling relation analysis does not rely on the absolute value of the fragment mass or migration time predicted by Equations (7) and (9), the straightforward use of Equation (7) indicates a fragmentation mass scale  $M_{\text{frag}} \sim 10^{-3} - 10^{-4} M_\odot$ . This is significantly below the mass of 2MASS J18082002–5104378 B, and the implication is that subsequent accretion was also important for its formation. Similarly, a simple ap-

plication of Equation (9) suggests a migration time that is an order of magnitude longer than that observed in the detailed hydrodynamic models of Hirano & Bromm (2017). Nevertheless, we argue that the advantage of a scaling analysis is that it bypasses these apparent normalization issues.

#### 4. DISCUSSION

2MASS J18082002–5104378 B is significantly lower in mass than all other known UMP stars. Because most metal-poor star surveys are effectively magnitude limited, most known metal-poor stars are giants, subgiants, or main sequence turnoff stars. Few are low-mass main sequence stars. Of all stars with  $[M/H] \leq -2.5$  in the JINABase (Abohalima & Frebel 2017) and the Stellar Abundances for Galactic Archaeology (SAGA; Suda et al. 2008, 2011; Yamada et al. 2013) databases, only 5/981 and 13/1314 have  $\log g \geq 4.0$  and  $T_{\text{eff}} \leq 5000$  K. The MIST isochrones indicate that at its mass, 2MASS J18082002–5104378 B has  $T_{\text{eff}} \approx 4200$  K,  $\log g \approx 5.2$ , bolometric luminosity  $L \approx 6.7 \times 10^{-3} L_\odot$ , and V-band absolute magnitude  $M_V \approx 10.8$ . At the distance of the 2MASS J18082002–5104378 system, it likely has an unreddened  $V \approx 19.7$ . Indeed, if 2MASS J18082002–5104378 B were a field star its ordinary proper motion and faint apparent magnitude would never attract attention.

Measured by its total mass in heavy elements, 2MASS J18082002–5104378 B is the most metal-poor star ever discovered. We calculated the total heavy element masses of 2MASS J18082002–5104378 B, HE 1523–0901 B, and every star in the JINABase and SAGA databases. We focused on the observable elements with logarithmic abundances  $\epsilon > 6$  according to Asplund et al.

(2009): carbon, nitrogen, oxygen, sodium, magnesium, aluminum, silicon, sulfur, calcium, iron, and nickel. Excluding the unobservable noble gases neon and argon, together these 11 elements comprise more than 99% of the metal mass of a solar-composition star. We assumed the standard atomic weights for each element and that each star in the JINAbase and SAGA samples has  $M_* = 0.8 M_\odot$ . We excluded upper limits and ignored missing elements when we summed the total metal mass of a star. We found that 2MASS J18082002–5104378 B has total metal mass of  $0.090 M_\oplus \approx 0.84 M_{\text{Mars}}$ . It has fewer grams of heavy elements than the next closest star SDSS J102915.14+172927.9 (Caffau et al. 2011, 2012), which has a total metal mass of  $0.10 M_\oplus \approx 1.1 M_{\text{Mars}}$ . The brown dwarf HE 1523–0901 B is even more extreme, as it has a total metal mass of only  $0.07 M_\oplus \approx 0.7 M_{\text{Mars}}$ . We plot in Figure 5 total metal mass as a function of  $[\text{Fe}/\text{H}]$  for 2MASS J18082002–5104378 B, HE 1523–0901 B, and every star in the JINAbase and SAGA databases.

The 2MASS J18082002–5104378 system is the most metal-poor star system on a thin disk orbit yet found. Its thin disk orbit is unusual for a metal-poor star, as only one out of 101 stars from Beers et al. (2017) with  $[\text{Fe}/\text{H}] \lesssim -2.5$  have similar Galactic orbital parameters. One problem with this simple analysis is that most searches for metal-poor stars avoid the plane of the Galaxy, so observational selection effects may have made it very difficult to discover similarly metal-poor stars with thin disk orbits in the past.

Given its thin disk orbit, the  $13.535 \pm 0.002$  Gyr age of the 2MASS J18082002–5104378 system provides a lower limit on the age of the thin disk. Similarly old but not quite as metal-poor stars have also been seen on thin disk orbits (e.g., Casagrande et al. 2011; Bensby et al. 2014). This is somewhat older than the 8–10 Gyr age of the thin disk suggested by classical studies of field stars (Edvardsson et al. 1993; Liu & Chaboyer 2000; Sandage et al. 2003), the white dwarf luminosity function (e.g., Oswalt et al. 1996; Leggett et al. 1998; Knox et al. 1999; Kilic et al. 2017), and the ages of the oldest disk open clusters Berkeley 17 and NGC 6791 (e.g., Krusberg & Chaboyer 2006; Brogaard et al. 2012).

While 2MASS J18082002–5104378 A is a subgiant and therefore likely to yield a reasonable isochrone-derived mass and age, our random mass and age uncertainties are probably too small. Both are almost certainly affected by significant systematic uncertainties. For example, the Dartmouth isochrone grid we fit to our observational data has not accounted for the possible non-solar carbon abundance of the 2MASS J18082002–5104378 system or the possibility that important stellar model parameters like mixing length may vary with compo-

sition (e.g., Bonaca et al. 2012; Metcalfe et al. 2014; Tayar et al. 2017; Joyce & Chaboyer 2018; Viani et al. 2018). Nevertheless, the low metallicity and ancient age of 2MASS J18082002–5104378 does suggest that the thin disk may be older than usually assumed.

Our conclusions about the likely formation of low-mass stars via disk fragmentation in primordial composition protostellar disks around Pop III stars support the fidelity of disk fragmentation events seen in recent numerical simulations of Pop III star formation (e.g., Clark et al. 2008, 2011a,b; Stacy et al. 2010, 2012, 2016; Greif et al. 2011, 2012; Dopcke et al. 2013; Stacy & Bromm 2013, 2014; Hirano & Bromm 2017; Riaz et al. 2018). At the resolutions necessary to observe fragmentation, these simulations can only be run for order 10 dynamical times, far too short a time to follow any possible migration of a newly formed fragment due to disk torques and evaluate its survival. Our scaling relation analysis of the 2MASS J18082002–5104378 and HE 1523–0901 systems implied that the migration times of fragments in Pop III disks with appropriately scaled masses should be longer than the disk migration times of 2MASS J18082002–5104378 B and HE 1523–0901 B. Therefore, since they both survived, fragments in primordial composition disks with migration times even longer could survive as well. We therefore argue that disk fragmentation is likely to form low-mass Pop III stars. We further suggest that at least some of those fragments are likely to survive as low-mass stars instead of merging with the primary forming at the center of their stellar system. These surviving low-mass Pop III stars would have main sequence lifetimes long enough that they could persist in our Galaxy to the present day.

## 5. CONCLUSION

We report the discovery of a low-mass secondary star in the 13.5 Gyr old,  $[\text{Fe}/\text{H}] \approx -4.1$  single-lined spectroscopic binary system 2MASS J18082002–5104378. The secondary star 2MASS J18082002–5104378 B has a mass  $M_2 = 0.14_{-0.01}^{+0.06} M_\odot$ , very close to the hydrogen-burning limit for its composition. It is the lowest-mass ultra metal-poor star currently known. Because of its low mass and metallicity, 2MASS J18082002–5104378 B has fewer grams of heavy elements than any other star currently known. Despite its age and metallicity, the 2MASS J18082002–5104378 system is on a thin disk like orbit. Indeed, it is the most metal-poor star system yet found to be kinematically associated with the thin disk. In concert with theoretical models of protostellar disks around both ultra metal-poor and primordial composition protostars, the observed properties

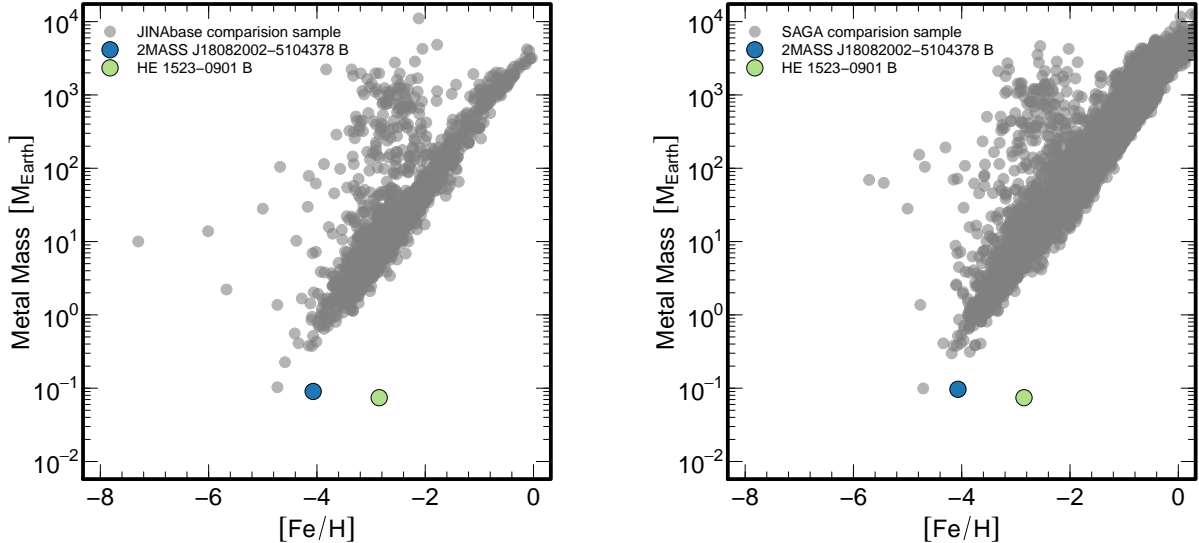


**Figure 5.** Total metal mass as a function of iron metallicity for known metal-poor stars. Left: comparison with the JINABase database. Right: comparison with the SAGA database. 2MASS J18082002–5104378 B has a total metallicity  $[M/H] \approx -3.84$  and a mass  $M_2 = 0.14_{-0.01}^{+0.06} M_\odot$ . Because of its low metallicity and mass, 2MASS J18082002–5104378 B has a total metal mass of only  $0.090 M_\oplus \approx 0.84 M_{\text{Mars}}$ , making it the most metal-poor star known. HE 1523–0901 B has a total metallicity  $[M/H] \approx -2.81$  and a mass  $M_2 = 0.011_{-0.001}^{+0.003} M_\odot = 11_{-1}^{+4} M_{\text{Jup}}$ . Because of its low metallicity and mass, HE 1523–0901 B has a total metal mass of only  $0.07 M_\oplus \approx 0.7 M_{\text{Mars}}$ . The uncertainties on the total metal masses of 2MASS J18082002–5104378 B and HE 1523–0901 B are smaller than the plotted points.

of 2MASS J18082002–5104378 B and the  $[Fe/H] \sim -3$  brown dwarf HE 1523–0901 B support the theoretically proposed idea that low-mass Pop III stars form via disk fragmentation. While low-mass Pop III star formation via disk fragmentation has been seen in numerical simulations, it is impossible to run those simulations long enough to verify that fragments survive disk migration. Our discovery reveals for the first time that fragments do survive the era of disk migration. This inference is independent of poorly modeled supernova yields or the possible atmospheric contamination of Pop III stars, two issues that have hindered past observational efforts to validate the existence of low-mass Pop III stars. Collectively, these results imply that low-mass Pop III stars formed via disk fragmentation can exist in our Galaxy.

We thank David Nataf, Brian O’Shea, and Jason Tumlinson for helpful comments. We are grateful to the anonymous referee for providing an extraordinarily quick and insightful referee report with several suggestions that improved the paper. A.R.C. is supported through an Australian Research Council Discovery Project under grant DP160100637. This paper includes data gathered with the 6.5 m Magellan Telescopes located at Las Campanas Observatory, Chile. Based on data obtained from the ESO Science Archive Facility under request number 270734. Based on observations collected at the European Organisation for As-

tronomical Research in the Southern Hemisphere under ESO programme 293.D-5036(A). Based on observations obtained under programs GS-2016A-Q-76, GS-2016B-Q-80, and GS-2017A-Q-66 at the Gemini Observatory, which is operated by the Association of Universities for Research in Astronomy, Inc., under a cooperative agreement with the NSF on behalf of the Gemini partnership: the National Science Foundation (United States), the National Research Council (Canada), CONICYT (Chile), Ministerio de Ciencia, Tecnología e Innovación Productiva (Argentina), and Ministério da Ciência, Tecnologia e Inovação (Brazil). This work has made use of data from the European Space Agency (ESA) mission *Gaia* (<https://www.cosmos.esa.int/gaia>), processed by the *Gaia* Data Processing and Analysis Consortium (DPAC, <https://www.cosmos.esa.int/web/gaia/dpac/consortium>). Funding for the DPAC has been provided by national institutions, in particular the institutions participating in the *Gaia* Multilateral Agreement. The national facility capability for SkyMapper has been funded through ARC LIEF grant LE130100104 from the Australian Research Council, awarded to the University of Sydney, the Australian National University, Swinburne University of Technology, the University of Queensland, the University of Western Australia, the University of Melbourne, Curtin University of Technology, Monash University and the Australian Astronomical Observatory. SkyMapper is owned and operated by

The Australian National University’s Research School of Astronomy and Astrophysics. The survey data were processed and provided by the SkyMapper Team at ANU. The SkyMapper node of the All-Sky Virtual Observatory (ASVO) is hosted at the National Computational Infrastructure (NCI). Development and support the SkyMapper node of the ASVO has been funded in part by Astronomy Australia Limited (AAL) and the Australian Government through the Commonwealth’s Education Investment Fund (EIF) and National Collaborative Research Infrastructure Strategy (NCRIS), particularly the National eResearch Collaboration Tools and Resources (NeCTAR) and the Australian National Data Service Projects (ANDS). This publication makes use of data products from the Two Micron All Sky Survey, which is a joint project of the University of Massachusetts and the Infrared Processing and Analysis Center/California Institute of Technology, funded by the National Aeronautics and Space Administration and the National Science Foundation. This publication makes use of data products from the *Wide-field Infrared Survey Explorer*, which is a joint project of the University of California, Los Angeles, and the Jet Propulsion Laboratory/California Institute of Technology, funded

by the National Aeronautics and Space Administration. This research was made possible through the use of the AAVSO Photometric All-Sky Survey (APASS), funded by the Robert Martin Ayers Sciences Fund. This research has made use of NASA’s Astrophysics Data System Bibliographic Services. This research made use of Astropy, a community-developed core Python package for Astronomy (Astropy Collaboration et al. 2013, 2018). This research has made use of the SIMBAD database, operated at CDS, Strasbourg, France (Wenger et al. 2000). This research has made use of the VizieR catalogue access tool, CDS, Strasbourg, France. The original description of the VizieR service was published in A&AS 143, 23 (Ochsenbein et al. 2000).

*Facilities:* Magellan:Clay (MIKE echelle spectrograph), VLT:Kueyen (UVES echelle spectrograph), Gemini:South (GMOS-S imaging spectrograph).

*Software:* `astropy` (Astropy Collaboration et al. 2013, 2018), `CarPy` (Kelson et al. 2000; Kelson 2003), `ExoFit` (Balan & Lahav 2009), `galpy` (Bovy 2015), `isochrones` (Morton 2015), `numpy` (Oliphant 2006), `MultiNest` (Feroz & Hobson 2008; Feroz et al. 2009, 2013), `pandas` (McKinney 2010), `R` (R Core Team 2018), `scipy` (Jones et al. 2001)

## REFERENCES

- Abel, T., Bryan, G. L., & Norman, M. L. 2000, *ApJ*, 540, 39
- Abel, T., Bryan, G. L., & Norman, M. L. 2002, *Science*, 295, 93
- Abohalima, A., & Frebel, A. 2017, arXiv:1711.04410
- Alpher, R. A., Bethe, H., & Gamow, G. 1948, *Physical Review*, 73, 803
- Aoki, W., Tominaga, N., Beers, T. C., Honda, S., & Lee, Y. S. 2014, *Science*, 345, 912
- Arenou, F., Luri, X., Babusiaux, C., et al. 2018, *A&A*, 616, A17
- Asplund, M., Grevesse, N., Sauval, A. J., & Scott, P. 2009, *ARA&A*, 47, 481
- Astropy Collaboration, Price-Whelan, A. M., Sipőcz, B. M., et al. 2018, *AJ*, 156, 123
- Astropy Collaboration, Robitaille, T. P., Tollerud, E. J., et al. 2013, *A&A*, 558, A33
- Balan, S. T., & Lahav, O. 2009, *MNRAS*, 394, 1936
- Baruteau, C., Meru, F., & Paardekooper, S.-J. 2011, *MNRAS*, 416, 1971
- Beers, T. C., & Christlieb, N. 2005, *ARA&A*, 43, 531
- Beers, T. C., Placco, V. M., Carollo, D., et al. 2017, *ApJ*, 835, 81
- Bensby, T., Feltzing, S., & Oey, M. S. 2014, *A&A*, 562, A71
- Bernstein, R., Shectman, S. A., Gunnels, S. M., Mochnacki, S., & Athey, A. E. 2003, *Proc. SPIE*, 4841, 1694
- Bland-Hawthorn, J., & Gerhard, O. 2016, *ARA&A*, 54, 529
- Bonaca, A., Tanner, J. D., Basu, S., et al. 2012, *ApJL*, 755, L12
- Bovy, J. 2015, *ApJS*, 216, 29
- Brogaard, K., VandenBerg, D. A., Bruntt, H., et al. 2012, *A&A*, 543, A106
- Bromm, V. 2013, *Reports on Progress in Physics*, 76, 112901
- Bromm, V., Coppi, P. S., & Larson, R. B. 1999, *ApJL*, 527, L5
- Bromm, V., Coppi, P. S., & Larson, R. B. 2002, *ApJ*, 564, 23
- Caffau, E., Bonifacio, P., François, P., et al. 2011, *Nature*, 477, 67
- Caffau, E., Bonifacio, P., François, P., et al. 2012, *A&A*, 542, A51
- Casagrande, L., Schönrich, R., Asplund, M., et al. 2011, *A&A*, 530, A138
- Chiaki, G., Yoshida, N., & Hirano, S. 2016, *MNRAS*, 463, 2781
- Choi, J., Dotter, A., Conroy, C., et al. 2016, *ApJ*, 823, 102



- Clark, P. C., Glover, S. C. O., & Klessen, R. S. 2008, *ApJ*, 672, 757
- Clark, P. C., Glover, S. C. O., Klessen, R. S., & Bromm, V. 2011a, *ApJ*, 727, 110
- Clark, P. C., Glover, S. C. O., Smith, R. J., et al. 2011b, *Science*, 331, 1040
- Coelho, P., Barbuy, B., Meléndez, J., Schiavon, R. P., & Castilho, B. V. 2005, *A&A*, 443, 735
- Cyburt, R. H., Fields, B. D., Olive, K. A., & Yeh, T.-H. 2016, *Reviews of Modern Physics*, 88, 015004
- da Silva, L., Girardi, L., Pasquini, L., et al. 2006, *A&A*, 458, 609
- de Bressan, M., Salvadori, S., Schneider, R., Valiante, R., & Omukai, K. 2017, *MNRAS*, 465, 926
- Dekker, H., D’Odorico, S., Kaufer, A., Delabre, B., & Kotzłowski, H. 2000, *Proc. SPIE*, 4008, 534
- Dopcke, G., Glover, S. C. O., Clark, P. C., & Klessen, R. S. 2013, *ApJ*, 766, 103
- Dotter, A. 2016, *ApJS*, 222, 8
- Dotter, A., Chaboyer, B., Jevremović, D., et al. 2007, *AJ*, 134, 376
- Dotter, A., Chaboyer, B., Jevremović, D., et al. 2008, *ApJS*, 178, 89
- Edvardsson, B., Andersen, J., Gustafsson, B., et al. 1993, *A&A*, 275, 101
- Evans, D. W., Riello, M., De Angeli, F., et al. 2018, *A&A*, 616, A4
- Feroz, F., & Hobson, M. P. 2008, *MNRAS*, 384, 449
- Feroz, F., Hobson, M. P., & Bridges, M. 2009, *MNRAS*, 398, 1601
- Feroz, F., Hobson, M. P., Cameron, E., & Pettitt, A. N. 2013, *arXiv:1306.2144*
- Fraser, M., Casey, A. R., Gilmore, G., Heger, A., & Chan, C. 2017, *MNRAS*, 468, 418
- Frebel, A., Johnson, J. L., & Bromm, V. 2009, *MNRAS*, 392, L50
- Gaia Collaboration, Brown, A. G. A., Vallenari, A., et al. 2018, *A&A*, 616, A1
- Gaia Collaboration, Prusti, T., de Bruijne, J. H. J., et al. 2016, *A&A*, 595, A1
- Gimeno, G., Roth, K., Chiboucas, K., et al. 2016, *Proc. SPIE*, 9908, 99082S
- Glover, S. 2013, in *The First Galaxies, Astrophysics and Space Science Library*, Vol. 396, ed. T. Wiklund, B. Mobasher, & V. Bromm (Berlin: Springer), 103
- Gravity Collaboration, Abuter, R., Amorim, A., et al. 2018, *A&A*, 615, L15
- Greif, T. H. 2015, *Computational Astrophysics and Cosmology*, 2, 3
- Greif, T. H., Bromm, V., Clark, P. C., et al. 2012, *MNRAS*, 424, 399
- Greif, T. H., Springel, V., White, S. D. M., et al. 2011, *ApJ*, 737, 75
- Halbwachs, J. L. 1987, *A&A*, 183, 234
- Hambly, N. C., Cropper, M., Boudreault, S., et al. 2018, *A&A*, 616, A15
- Hansen, T. T., Andersen, J., Nordström, B., et al. 2015, *A&A*, 583, A49
- Hartwig, T., Bromm, V., Klessen, R. S., & Glover, S. C. O. 2015, *MNRAS*, 447, 3892
- Henden, A. A., Templeton, M., Terrell, D., et al. 2016, *yCat*, 2336, 0
- Hirano, S., & Bromm, V. 2017, *MNRAS*, 470, 898
- Hirano, S., Hosokawa, T., Yoshida, N., Omukai, K., & Yorke, H. W. 2015, *MNRAS*, 448, 568
- Hirano, S., Hosokawa, T., Yoshida, N., et al. 2014, *ApJ*, 781, 60
- Hogeveen, S. J. 1992, *Ap&SS*, 194, 143
- Hook, I. M., Jørgensen, I., Allington-Smith, J. R., et al. 2004, *PASP*, 116, 425
- Hosokawa, T., Hirano, S., Kuiper, R., et al. 2016, *ApJ*, 824, 119
- Hosokawa, T., Omukai, K., Yoshida, N., & Yorke, H. W. 2011, *Science*, 334, 1250
- Ishigaki, M. N., Tominaga, N., Kobayashi, C., & Nomoto, K. 2018, *ApJ*, 857, 46
- Johnson, J. L. 2015, *MNRAS*, 453, 2771
- Jones, E., Oliphant, E., & Peterson, P., *SciPy: Open Source Scientific Tools for Python*, 2001, <http://www.scipy.org/>
- Joyce, M., & Chaboyer, B. 2018, *ApJ*, 856, 10
- Jurić, M., Ivezić, Ž., Brooks, A., et al. 2008, *ApJ*, 673, 864
- Kelson, D. D. 2003, *PASP*, 115, 688
- Kelson, D. D., Illingworth, G. D., van Dokkum, P. G., & Franx, M. 2000, *ApJ*, 531, 137
- Kilic, M., Munn, J. A., Harris, H. C., et al. 2017, *ApJ*, 837, 162
- Komiya, Y., Suda, T., & Fujimoto, M. Y. 2015, *ApJL*, 808, L47
- Komiya, Y., Suda, T., & Fujimoto, M. Y. 2016, *ApJ*, 820, 59
- Knox, R. A., Hawkins, M. R. S., & Hambly, N. C. 1999, *MNRAS*, 306, 736
- Kratzer, K., & Lodato, G. 2016, *ARA&A*, 54, 271
- Krusberg, Z. A. C., & Chaboyer, B. 2006, *AJ*, 131, 1565
- Leggett, S. K., Ruiz, M. T., & Bergeron, P. 1998, *ApJ*, 497, 294
- Lindegren, L., Hernández, J., Bombrun, A., et al. 2018, *A&A*, 616, A2
- Liu, W. M., & Chaboyer, B. 2000, *ApJ544*, 818

- Luri, X., Brown, A. G. A., Sarro, L. M., et al. 2018, *A&A*, 616, A9
- Mainzer, A., Bauer, J., Grav, T., et al. 2011, *ApJ*, 731, 53
- McKee, C. F., & Tan, J. C. 2008, *ApJ*, 681, 771
- McKinney, W. 2010, Proc. IX Python in Science Conf., ed. S. van der Walt & J. Millman (Austin, TX: SciPy), 51, <http://conference.scipy.org/proceedings/scipy2010/>
- Meléndez, J., Placco, V. M., Tucci-Maia, M., et al. 2016, *A&A*, 585, L5
- Metcalfe, T. S., Creevey, O. L., Doğan, G., et al. 2014, *ApJS*, 214, 27
- Miyamoto, M., & Nagai, R. 1975, *PASJ*, 27, 533
- Morton, T. D. 2015, Isochrones: Stellar Model Grid Package, Astrophysics Source Code Library, ascl:1503.010
- Navarro, J. F., Frenk, C. S., & White, S. D. M. 1996, *ApJ*, 462, 563
- O’Shea, B. W., & Norman, M. L. 2007, *ApJ*, 654, 66
- Ochsenbein, F., Bauer, P., & Marcout, J. 2000, *A&AS*, 143, 23
- Oliphant, T. E. 2006, *A Guide to NumPy* (Spanish Fork, UT: Trelgol Publishing)
- Oswalt, T. D., Smith, J. A., Wood, M. A., & Hintzen, P. 1996, *Nature*, 382, 692
- Paardekooper, S.-J., & Johansen, A. 2018, *SSRv*, 214, 38
- Paxton, B., Bildsten, L., Dotter, A., et al. 2011, *ApJS*, 192, 3
- Paxton, B., Cantiello, M., Arras, P., et al. 2013, *ApJS*, 208, 4
- Paxton, B., Marchant, P., Schwab, J., et al. 2015, *ApJS*, 220, 15
- Placco, V. M., Frebel, A., Lee, Y. S., et al. 2015, *ApJ*, 809, 136
- R Core Team 2018, *R: A Language and Environment for Statistical Computing* (Vienna: R Foundation for Statistical Computing)
- Riaz, R., Bovino, S., Vanaverbeke, S., & Schleicher, D. R. G. 2018, *MNRAS*, 479, 667
- Riello, M., De Angeli, F., Evans, D. W., et al. 2018, *A&A*, 616, A3
- Salgado, J., González-Núñez, J., Gutiérrez-Sánchez, R., et al. 2017, *Astronomy and Computing*, 21, 22
- Salvadori, S., Schneider, R., & Ferrara, A. 2007, *MNRAS*, 381, 647
- Sandage, A., Lubin, L. M., & Vandenberg, D. A. 2003, *PASP*, 115, 1187
- Saumon, D., Bergeron, P., Lunine, J. I., Hubbard, W. B., & Burrows, A. 1994, *ApJ*, 424, 333
- Schneider, R., Omukai, K., Bianchi, S., & Valiante, R. 2012, *MNRAS*, 419, 1566
- Shakura, N. I., & Sunyaev, R. A. 1973, *A&A*, 24, 337
- Shectman, S. A., & Johns, M. 2003, *Proc. SPIE*, 4837, 910
- Shen, S., Kulkarni, G., Madau, P., & Mayer, L. 2017, *MNRAS*, 469, 4012
- Silk, J. 1983, *MNRAS*, 205, 705
- Skrutskie, M. F., Cutri, R. M., Stiening, R., et al. 2006, *AJ*, 131, 1163
- Soubiran, C., Jasniewicz, G., Chemin, L., et al. 2013, *A&A*, 552, A64
- Stacy, A., & Bromm, V. 2013, *MNRAS*, 433, 1094
- Stacy, A., & Bromm, V. 2014, *ApJ*, 785, 73
- Stacy, A., Bromm, V., & Lee, A. T. 2016, *MNRAS*, 462, 1307
- Stacy, A., Greif, T. H., & Bromm, V. 2010, *MNRAS*, 403, 45
- Stacy, A., Greif, T. H., & Bromm, V. 2012, *MNRAS*, 422, 290
- Suda, T., Katsuta, Y., Yamada, S., et al. 2008, *PASJ*, 60, 1159
- Suda, T., Yamada, S., Katsuta, Y., et al. 2011, *MNRAS*, 412, 843
- Susa, H. 2013, *ApJ*, 773, 185
- Susa, H., Hasegawa, K., & Tominaga, N. 2014, *ApJ*, 792, 32
- Takahashi, K., Umeda, H., & Yoshida, T. 2014, *ApJ*, 794, 40
- Takahashi, K., Yoshida, T., & Umeda, H. 2018, *ApJ*, 857, 111
- Tanaka, K. E. I., & Omukai, K. 2014, *MNRAS*, 439, 1884
- Tanaka, S. J., Chiaki, G., Tominaga, N., & Susa, H. 2017, *ApJ*, 844, 137
- Tanikawa, A., Suzuki, T. K., & Doi, Y. 2018, *PASJ*, 70, 80
- Tayar, J., Somers, G., Pinsonneault, M. H., et al. 2017, *ApJ*, 840, 17
- Tegmark, M., Silk, J., Rees, M. J., et al. 1997, *ApJ*, 474, 1
- Tody, D. 1986, *Proc. SPIE*, 627, 733
- Tody, D. 1993, *adass II*, 52, 173
- Tominaga, N., Iwamoto, N., & Nomoto, K. 2014, *ApJ*, 785, 98
- Tonry, J., & Davis, M. 1979, *AJ*, 84, 1511
- Tumlinson, J. 2006, *ApJ*, 641, 1
- Turk, M. J., Abel, T., & O’Shea, B. 2009, *Science*, 325, 601
- Viani, L. S., Basu, S., Joel Ong J., M., Bonaca, A., & Chaplin, W. J. 2018, *ApJ*, 858, 28
- Vorobyov, E. I., DeSouza, A. L., & Basu, S. 2013, *ApJ*, 768, 131
- Wenger, M., Ochsenbein, F., Egret, D., et al. 2000, *A&AS*, 143, 9
- Wolf, C., Onken, C. A., Luvaul, L. C., et al. 2018, *PASA*, 35, e010
- Wright, E. L., Eisenhardt, P. R. M., Mainzer, A. K., et al. 2010, *AJ*, 140, 1868

Yamada, S., Suda, T., Komiya, Y., Aoki, W., & Fujimoto,  
M. Y. 2013, MNRAS, 436, 1362

Yoshida, N., Omukai, K., Hernquist, L., & Abel, T. 2006,  
ApJ, 652, 6